



This is a repository copy of *Three-dimensional millimetre-wave beam tracking based on smart phone sensor measurements and direction of arrival/time of arrival estimation for 5G networks*.

White Rose Research Online URL for this paper:
<http://eprints.whiterose.ac.uk/129293/>

Version: Accepted Version

Article:

Qi, Z. and Liu, W. orcid.org/0000-0003-2968-2888 (2018) Three-dimensional millimetre-wave beam tracking based on smart phone sensor measurements and direction of arrival/time of arrival estimation for 5G networks. *IET Microwaves, Antennas & Propagation*, 12 (3). pp. 271-279. ISSN 1751-8725

<https://doi.org/10.1049/iet-map.2017.0329>

Reuse

Unless indicated otherwise, fulltext items are protected by copyright with all rights reserved. The copyright exception in section 29 of the Copyright, Designs and Patents Act 1988 allows the making of a single copy solely for the purpose of non-commercial research or private study within the limits of fair dealing. The publisher or other rights-holder may allow further reproduction and re-use of this version - refer to the White Rose Research Online record for this item. Where records identify the publisher as the copyright holder, users can verify any specific terms of use on the publisher's website.

Takedown

If you consider content in White Rose Research Online to be in breach of UK law, please notify us by emailing eprints@whiterose.ac.uk including the URL of the record and the reason for the withdrawal request.



eprints@whiterose.ac.uk
<https://eprints.whiterose.ac.uk/>

Three-Dimensional Millimetre Wave Beam Tracking Based on Smart Phone Sensor Measurements and DOA/TOA Estimation for 5G Networks

 ISSN 1751-8644
 doi: 0000000000
 www.ietdl.org

Zichen Qi Wei Liu

 Communications Research Group, Department of Electronic and Electrical Engineering
 University of Sheffield, Sheffield S1 4ET, United Kingdom E-mail: {zqi2, w.liu}@sheffield.ac.uk

Abstract: The narrow millimetre wave beam in future 5G networks is easily interrupted by the movement of mobile handsets including both location change and self-rotation. In this paper, a three-dimensional (3-D) beam tracking method is proposed to achieve beam alignment between the access node (AN) and the user node (UN). A gradient descent algorithm is employed for self-rotation tracking based on measurements obtained by the three smart phone sensors (gyroscope, accelerometer and magnetometer) embedded in the micro-electro-mechanical system (MEMS). An extended Kalman filtering (EKF) based location tracking algorithm is also incorporated into the design by combining the data from direction of arrival (DoA) and time of arrival (ToA) estimation results of the user node (UN), since accurate UN location information is also crucial in the beam tracking process. Moreover, an operation protocol is developed to coordinate the tracking process and tested in different scenarios.

1 Introduction

In 5G ultra dense networks, it is envisaged that the distance between the various access nodes (ANs) and user nodes (UNs) would be in the range of tens of metres or even less. As a result, UNs are mainly in the line of sight (LoS) communications with ANs [1]. However, due to the inherent property of millimetre wave for transmission and reception, the beam alignment between the AN and the UN can be easily destroyed by even a slight movement of the UN, causing a significant loss of the received signal power. Therefore, the user's behavioral changes (self-rotation) and location information are essential for maintaining an acceptable level of the communication link between the AN and the UN.

However, traditional commercial positioning techniques may not meet the requirements of 5G beam tracking, including the global navigation satellite systems (GNSSs) with a root mean square error (RMSE) of 5m [2], LTE observed time difference of arrival (OTDoA) with an RMSE of about 25m [3], and WLAN fingerprinting of about 3m to 4m [4]. Fortunately, the extremely short wavelength of millimeter wave renders installation of a large number of antenna arrays at both UNs and ANs possible, and the wide bandwidth can lead to highly accurate position measurements such as ToA (time of arrival) and TDoA (time difference of arrival) [2]. In [5], a joint DoA/ToA tracking method based on extended Kalman filtering (EKF) and a clock offset positioning method was proposed with an accuracy of about 0.1m. By combining DoA and RSS (received signal strength), a low-complexity localization system was presented in [6]. Furthermore, the angle information acquired from DoA is applied in direction lock loop for tracking purposes in [7].

On the other hand, for 5G millimetre wave beam tracking, only a few research results have been reported in the literature. In [8], a method for tracking the signal to noise ratio (SNR) of the channel with prediction and detection was proposed. In [9], the effect of circular motion of the devices at 60GHz was studied. The experimental results of beam tracking for the base station in an indoor environment were presented in [10]. Moreover, a Kalman filter based beam tracking method with mobile sensors was introduced in [11]. As an extension to [11], a three-dimensional (3-D) millimeter wave beam tracking method based on sensor fusion and extended Kalman filter was proposed with different scenarios examined in [12]. The results

were only justified with the UN standing still at the same location. Also, the EKF applied in this paper requires complicated calculations, which would increase the workload of the smart phone and the network, as can be seen from the implementation in [13] and [14].

In this paper, as an expanded version of the work in [12], a new (3-D) tracking method is proposed to maintain the beam alignment between the AN and the UN in the 5G network using sensors embedded in smart phones. Compared to the work in [12], a gradient descent algorithm for rotation tracking based on [15] is applied in replace of EKF, which is a computationally efficient algorithm [15] and can achieve almost the same as or even better performance than the EKF with less computational complexity, and the proposed method is studied in more complicated scenarios, where a single user in an ultra-dense network with an LOS communication link moves in different situations. More specifically, a combination of DoA and ToA with extended Kalman filtering is used for location tracking; a uniform rectangular array (URA) is employed at the UN for 3-D beamforming and its main beam is adjusted towards the signal direction whenever it is below a preset threshold value; beam steering is employed for better performance instead of the fixed beam switching scheme adopted in [11]. For tracking behavioral changes (self-rotation) of the UN, we use the IMU (inertial measurement unit) of the smart phone to give self-measurements of the moving device. An IMU includes a three-axis gyroscope (for measuring of angular velocity), a three-axis accelerometer (for acceleration measurement), and a three-axis magnetometer (for magnetic field measurement), which are embedded in the micro-electro-mechanical system (MEMS) inside the smart phone. The data obtained from these sensors are incorporated by the gradient descent algorithm for tracking behavioral changes of the UN, where the gyroscope gives state update, while accelerometer and magnetometer provide measurement update to correct the gyroscope drift error. Besides, a protocol is proposed to give specific instructions for the method to be implemented at the network and device level.

This paper is organized as follows. The self-rotation tracking method for the smart phone is presented in Sec. 2, while localization and tracking of the UN is introduced in Sec. 3. The proposed overall tracking algorithm is described in Sec. 4. Simulation results are provided in Sec. 5, and conclusions are drawn in Sec. 6.

2 Self-Rotation Tracking

2.1 Quaternion Representation

Quaternion algebra is widely used for defining the orientation of a rigid body coordinated frame in a 3-D space. An arbitrary axis in frame n can be calculated through a rotation around a vector defined in frame k . The quaternion representing the orientation ${}^n_k\hat{\mathbf{q}}$ can be defined by equation (1), where r_x , r_y and r_z describe the components of unit vector in frame n .

$${}^n_k\hat{\mathbf{q}} = [q_1 \quad q_2 \quad q_3 \quad q_4] = \begin{bmatrix} \cos(\frac{\alpha}{2}) \\ -r_x * \sin(\frac{\alpha}{2}) \\ -r_y * \sin(\frac{\alpha}{2}) \\ -r_z * \sin(\frac{\alpha}{2}) \end{bmatrix}^T \quad (1)$$

The quaternion conjugate, denoted by $*$, is defined as

$${}^n_k\hat{\mathbf{q}}^* = {}^k_n\hat{\mathbf{q}} = \begin{bmatrix} q_1 \\ -q_2 \\ -q_3 \\ -q_4 \end{bmatrix}^T \quad (2)$$

The vector expressed in frame n can be switched to frame k through the following equation:

$$\mathbf{v}^k = {}^n_k\hat{\mathbf{q}} \otimes \mathbf{v}^n {}^n_k\hat{\mathbf{q}}^* \quad (3)$$

The quaternion product, denoted by \otimes , is an operation for multiple rotations. For example, rotation from frame n to frame i can be achieved through the product of ${}^k_i\hat{\mathbf{q}}$ and ${}^n_k\hat{\mathbf{q}}$ in equation (4) to give the transformation quaternion ${}^n_i\hat{\mathbf{q}}$. Therefore, any vectors expressed in frame n can be changed to i by multiplying with ${}^n_i\hat{\mathbf{q}}$.

$${}^n_i\hat{\mathbf{q}} = {}^k_i\hat{\mathbf{q}} \otimes {}^n_k\hat{\mathbf{q}} \quad (4)$$

The operation of quaternions \mathbf{X} and \mathbf{Y} 's product is under the Hamilton rule and is not commutative [16].

$$\mathbf{X} \otimes \mathbf{Y} = \begin{bmatrix} x_1 \\ x_2 \\ x_3 \\ x_4 \end{bmatrix}^T \otimes \begin{bmatrix} y_1 \\ y_2 \\ y_3 \\ y_4 \end{bmatrix}^T = \begin{bmatrix} x_1y_1 - x_2y_2 - x_3y_3 - x_4y_4 \\ x_1y_2 + x_2y_1 + x_3y_4 - x_4y_3 \\ x_1y_3 - x_2y_4 + x_3y_1 + x_4y_2 \\ x_1y_4 + x_2y_3 - x_3y_2 + x_4y_1 \end{bmatrix}^T \quad (5)$$

2.2 Euler Angles and Coordinates Transform

The popular rotation angle set of yaw(γ)-pitch(β)-roll(α) (also expressed in z-y-x form) is chosen and rotation can be expressed as a sequence with initial status $z_0 - y_0 - x_0$, first rotation $z_1 - y_1 - x_1$, second rotation $z_2 - y_2 - x_2$, and final rotation $z_3 - y_3 - x_3$. The three rotation processes can be represented individually in the form of the Direction Cosine Matrix (DCM) or the rotation matrix as three basic clockwise rotations.

A yaw rotation around the z-axis is defined as

$$\mathbf{R}_z(\gamma) = \begin{bmatrix} \cos \gamma & -\sin \gamma & 0 \\ \sin \gamma & \cos \gamma & 0 \\ 0 & 0 & 1 \end{bmatrix}. \quad (6)$$

A pitch rotation around the y-axis is defined as

$$\mathbf{R}_y(\beta) = \begin{bmatrix} \cos \beta & 0 & \sin \beta \\ 0 & 1 & 0 \\ -\sin \beta & 0 & \cos \beta \end{bmatrix}. \quad (7)$$

A roll rotation around the x-axis is defined as

$$\mathbf{R}_x(\alpha) = \begin{bmatrix} 1 & 0 & 0 \\ 0 & \cos \alpha & -\sin \alpha \\ 0 & \sin \alpha & \cos \alpha \end{bmatrix}. \quad (8)$$

A combination of the three DCMs is often used to represent more complicated rotations :

$$\mathbf{R} = \begin{bmatrix} \cos \beta \cos \gamma & & & \\ \sin \alpha \sin \beta \cos \gamma - \cos \alpha \sin \beta & & & \\ \cos \alpha \sin \beta \cos \gamma + \sin \alpha \sin \beta & & & \\ & \cos \beta \sin \gamma & -\sin \beta & \\ & \sin \alpha \sin \beta \sin \gamma + \cos \alpha \cos \gamma & \sin \alpha \cos \beta & \\ & \cos \alpha \sin \beta \sin \gamma - \sin \alpha \cos \gamma & \cos \alpha \cos \beta & \end{bmatrix} \quad (9)$$

Moreover, the orientation described by a quaternion can be represented as the rotation matrix through the following equation

$$\mathbf{R} = \begin{bmatrix} 2q_1^2 - 1 + 2q_2^2 & & & \\ 2(q_2q_3 - q_1q_4) & & & \\ 2(q_2q_4 + q_1q_3) & & & \\ & 2(q_2q_3 + q_1q_4) & 2(q_2q_4 - q_1q_3) & \\ & 2q_1^2 - 1 + 2q_3^2 & 2(q_3q_4 + q_1q_2) & \\ & 2(q_2q_4 - q_1q_2) & 2q_1^2 - 1 + 2q_4^2 & \end{bmatrix} \quad (10)$$

The Euler angles can be described by equations (11), (12) and (13) in the quaternion form.

$$\gamma = \text{Atan2}(2q_2q_3 - 2q_1q_4, 2q_1^2 + 2q_2^2 - 1) \quad (11)$$

$$\beta = -\sin^{-1}(2q_2q_4 + 2q_1q_3) \quad (12)$$

$$\alpha = \text{Atan2}(2q_3q_4 - 2q_1q_2, 2q_1^2 + 2q_4^2 - 1) \quad (13)$$

and atan2 is a four-quadrant inverse tangent function [17]:

$$\text{atan2}(y, x) = \begin{cases} \arctan \frac{y}{x} & \text{if } x > 0, \\ \frac{\pi}{2} - \arctan \frac{x}{y} & \text{if } y > 0, \\ -\frac{\pi}{2} - \arctan \frac{x}{y} & \text{if } y < 0, \\ -\arctan \frac{y}{x} + / - \pi & \text{if } x < 0, \\ \text{undefined} & \text{if } x = y = 0, \end{cases} \quad (14)$$

K ANs are considered in an ultra-dense network for UN positioning. The location $P_{a,k} = (x_{a,k}, y_{a,k}, z_{a,k})$ of each AN defined in north-east-down (NED) local-level frame (LLF) is assumed to be known in advance with $k = 1, 2, \dots, K$ and UN is defined in the rigid body frame of the smart phone. In the process of position tracking using EKF [18], the UN sends a pilot signal periodically to communicate with the ANs. Thereafter, measurements from ToA and DoA are gathered by the network to yield a UN position estimate.

The location information of the UN $P_{u,k} = (x_{u,k}, y_{u,k}, z_{u,k})$, $k = 1, 2, \dots, K$, is also defined in NED. Thus, the line of sight vector, \mathbf{l}_l , is calculated as (15), where l represents line of sight.

$$\mathbf{l}_l = P_{u,k} - P_{a,k} \quad (15)$$

so $\mathbf{l}_l = [x_{u,k} - x_{a,k} \quad y_{u,k} - y_{a,k} \quad z_{u,k} - z_{a,k}]^T$ and the LoS vector can be expressed by the Euler angle as follows, where b represents body frame.

$$\mathbf{l}_b = \mathbf{R}_l^b \mathbf{l}_b^l. \quad (16)$$

2.3 Tracking from the Sensors

There are three sensors embedded in a smart phone: a three-axis gyroscope, a three-axis accelerometer and a three-axis magnetometer. Although the gyroscope itself can measure the three rotation angles (yaw, pitch, and roll) accurately in short time, the drift error caused by integration could lead to significant errors in rotation tracking [19]. Besides, neither magnetometer nor accelerometer can

give reliable measurements. As a result, measurements from the three sensors have to be combined by a gradient descent algorithm to achieve a relatively high accuracy in rotation angle tracking. In detail, the quaternion estimation obtained from the gyroscope is corrected by quaternion-valued data obtained by the algorithm from the accelerometer and magnetometer.

The output of the gyroscope is angular velocity. It can be expressed as follows in the quaternion form

$$\boldsymbol{\omega} = [0 \quad \omega_x \quad \omega_y \quad \omega_z] \quad (17)$$

In the algorithm, the Earth's field is known in the global frame, and measurement of the relationship between the global frame and the rigid body frame is needed to compute the rotation. The rotation data from the gyroscope at time t can be calculated by numerically integrating the quaternion derivative $\dot{\hat{\mathbf{q}}}_{g,t}$ through equations (18) and (19).

$${}^B_G \dot{\hat{\mathbf{q}}}_{g,t} = \frac{1}{2} {}^B_G \hat{\mathbf{q}}_{est,t-1} \otimes \boldsymbol{\omega}_t \quad (18)$$

$${}^B_G \hat{\mathbf{q}}_{g,t} = {}^B_G \hat{\mathbf{q}}_{est,t-1} + {}^B_G \dot{\hat{\mathbf{q}}}_{g,t} \Delta t \quad (19)$$

In the above equations, ${}^B_G \hat{\mathbf{q}}_{g,t}$ is the rotation of the smart phone measured at time t , Δt is the sampling period and ${}^B_G \hat{\mathbf{q}}_{est,t-1}$ is the previously estimated orientation, where $\{\}$ indicates a normalized vector of unit length, and B and G represent the rigid body frame and the global frame, respectively.

The three-axis accelerometer measures the acceleration of each axis and transforms the data into roll and pitch angles. The yaw angle (rotation around the z-axis) cannot be determined from the accelerometer [19]. The gravity information needs to be subtracted from the model. The quaternion representation is used to compute the roll and pitch angle.

The output of the accelerometer is given by equation (20). The objective function and Jacobian equation can be defined through (21), (22) and (23), where ${}^B_G \hat{\mathbf{q}}$ is the frame transformation quaternion.

$$\mathbf{a}\hat{\mathbf{c}}\mathbf{c} = [0 \quad a_x \quad a_y \quad a_z] \quad (20)$$

$${}^B_G \hat{\mathbf{q}} = [q_1 \quad q_2 \quad q_3 \quad q_4] \quad (21)$$

$$\mathbf{W}_{acc}({}^B_G \hat{\mathbf{q}}, \mathbf{a}\hat{\mathbf{c}}\mathbf{c}) = \begin{bmatrix} 2(q_2q_4 - q_1q_3) - a_x \\ 2(q_1q_2 + q_3q_4) - a_y \\ 2(\frac{1}{2} - q_2^2 - q_3^2) - a_z \end{bmatrix} \quad (22)$$

$$\mathbf{Z}_{acc}({}^B_G \hat{\mathbf{q}}) = \begin{bmatrix} -2q_3 & 2q_4 & -2q_1 & 2q_2 \\ 2q_2 & 2q_1 & 2q_4 & 2q_3 \\ 0 & -4q_2 & -4q_3 & 0 \end{bmatrix} \quad (23)$$

The magnetometer measures the magnetic field. However, the magnetometer can be easily affected by other magnetic fields [19]. The Earth magnetic field can be considered to have two components: the vertical component and the horizontal component, which are represented in equation (25). The output of the magnetometer measurement is given in (24). The objective function and Jacobian equation are defined in (26) and (27). The magnetic distortion is compensated by (28) and (29), where \mathbf{c}_t is the compensated Earth magnetic field at time instant t .

$$\mathbf{m}\hat{\mathbf{a}}\mathbf{g} = [0 \quad b_x \quad b_y \quad b_z] \quad (24)$$

$$\mathbf{b}_e = [0 \quad b_{ex} \quad 0 \quad b_{ez}] \quad (25)$$

$$\mathbf{W}_{mag}({}^B_G \hat{\mathbf{q}}, \mathbf{b}_e, \mathbf{m}\hat{\mathbf{a}}\mathbf{g}) = \begin{bmatrix} 2b_{ex}(0.5 - q_3^2 - q_4^2) + \\ 2b_{ex}(q_2q_3 - q_1q_4) + \\ 2b_{ex}(q_1q_3 + q_2q_4) \\ 2b_{ez}(q_2q_4 - q_1q_3) - b_x \\ 2b_{ez}(q_1q_2 + q_3q_4) - b_y \\ 2b_{ez}(0.5 - q_2^2 - q_3^2) - b_z \end{bmatrix} \quad (26)$$

$$\mathbf{Z}_{mag}({}^B_G \hat{\mathbf{q}}, \mathbf{b}_e) = \begin{bmatrix} -2b_{ex}q_3 & 2b_{ez}q_4 \\ -2b_{ex}q_4 + 2b_{ez} & 2b_{ex}q_3 + 2b_{ez}q_1 \\ 2b_{ex} & 2b_{ex} - 4b_{ez}q_2 \\ -4b_{ex}q_3 - 2b_{ez}q_1 & -4b_{ex}q_4 + 2b_{ez}q_2 \\ 2b_{ex}q_2 + 2b_{ez}q_4 & -2b_{ex}q_1 + 2b_{ez}q_3 \\ 2b_{ex}q_1 - 4b_{ez}q_3 & 2b_{ex}q_2 \end{bmatrix} \quad (27)$$

$$\hat{\mathbf{n}}_t = [0 \quad n_x \quad n_y \quad n_z] = {}^B_G \hat{\mathbf{q}}_{est,t-1} \otimes \mathbf{m}\hat{\mathbf{a}}\mathbf{g} \otimes {}^B_G \hat{\mathbf{q}}_{est,t-1}^* \quad (28)$$

$$\mathbf{c}_t = [0 \quad \sqrt{n_x^2 + n_y^2} \quad 0 \quad n_z] \quad (29)$$

The data from the accelerometer and magnetometer is combined by equations (30) and (31) and substituting \mathbf{b}_e with \mathbf{c}_t .

$$\mathbf{W}_{acc,mag}({}^B_G \hat{\mathbf{q}}, \mathbf{a}\hat{\mathbf{c}}\mathbf{c}, \hat{\mathbf{c}}_t, \mathbf{m}\hat{\mathbf{a}}\mathbf{g}) = \begin{bmatrix} \mathbf{W}_{acc}({}^B_G \hat{\mathbf{q}}, \mathbf{a}\hat{\mathbf{c}}\mathbf{c}) \\ \mathbf{W}_{mag}({}^B_G \hat{\mathbf{q}}, \hat{\mathbf{c}}_t, \mathbf{m}\hat{\mathbf{a}}\mathbf{g}) \end{bmatrix} \quad (30)$$

$$\mathbf{Z}_{acc,mag}({}^B_G \hat{\mathbf{q}}, \hat{\mathbf{c}}_t) = \begin{bmatrix} \mathbf{Z}_{acc}^T({}^B_G \hat{\mathbf{q}}) \\ \mathbf{Z}_{mag}^T({}^B_G \hat{\mathbf{q}}, \hat{\mathbf{c}}_t) \end{bmatrix} \quad (31)$$

The process of the gradient descent algorithm is shown as follows, where ∇ represents the gradient operation and β is the magnitude of the error of the gyroscope measurement:

$${}^B_G \hat{\mathbf{q}}_{est,t} = {}^B_G \hat{\mathbf{q}}_{est,t-1} + {}^B_G \dot{\hat{\mathbf{q}}}_{est,t} \Delta t \quad (32)$$

$${}^B_G \dot{\hat{\mathbf{q}}}_{est,t} = {}^B_G \dot{\hat{\mathbf{q}}}_{g,t} - \beta \frac{\nabla f}{\|\nabla f\|} \quad (33)$$

$$\nabla f = \begin{cases} \mathbf{Z}_{acc}^T({}^B_G \hat{\mathbf{q}}_{est,t-1}) \mathbf{W}_{acc}({}^B_G \hat{\mathbf{q}}_{est,t-1}, \mathbf{a}\hat{\mathbf{c}}\mathbf{c}_t) \\ \mathbf{Z}_{acc,mag}^T({}^B_G \hat{\mathbf{q}}_{est,t-1}, \hat{\mathbf{c}}_t) \\ \Rightarrow \mathbf{W}_{acc,mag}({}^B_G \hat{\mathbf{q}}_{est,t-1}, \mathbf{a}\hat{\mathbf{c}}\mathbf{c}_t, \hat{\mathbf{c}}_t, \mathbf{m}\hat{\mathbf{a}}\mathbf{g}_t) \end{cases} \quad (34)$$

Fig.1 shows a flowchart of the gradient descent algorithm.

3 Localization and Tracking of the UN

3.1 Localization and Tracking Algorithm

Different from the tracking method employing several ANs in [18], we assume the UN communicates with only one base station at each time, since a single AN with TOA/DOA method in 5G ultra-dense networks is sufficient for the tracking process.

The state vector of a UN is defined as $\mathbf{s}[i] = [x[i], y[i], z[i], \dot{x}[i], \dot{y}[i], \dot{z}[i]]^T$ which evolves from the dynamic model

$$\mathbf{s}[i] = f(\mathbf{s}[i-1]) \quad (35)$$

where $\mathbf{s}[i]$ consists of the UN's location and velocity state at time step i changing with the function $f(\cdot)$ with covariance matrix \mathbf{Q} .

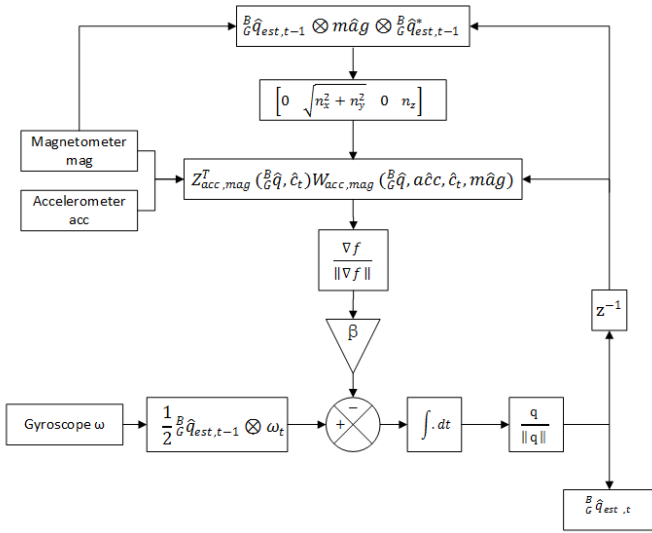


Fig. 1: Flowchart of the gradient descent algorithm.

The measurement equation is composed of the DoA and ToA of the k th AN, which are modelled as

$$\begin{aligned}\hat{a}_k[i] &= a_k[i] + e_{a,k}[i] \\ \hat{t}_k[i] &= t_k[i] + e_{t,k}[i],\end{aligned}\quad (36)$$

respectively, with estimation errors $e_{a,k}$ and $e_{t,k}$, where $a_k[i]$ denotes the 2-D DoA angle θ and ϕ . Hence, the measurement vector is written with the link to the state vector as

$$\mathbf{y}_k = [\hat{a}_k[i], \hat{t}_k[i]]^T = \mathbf{h}_k(s[i]) + \mathbf{m}_k[i] \quad (37)$$

where $\mathbf{h}_k(\cdot)$ is the handling function, and $\mathbf{m}_k[i] = [e_{a,k}[i], e_{t,k}[i]]^T$ with a noise covariance matrix \mathbf{R}_k . The relationship between the state vector and the measurement vector is

$$\hat{t}_k[i] = \frac{\sqrt{\Delta^2 x_k[i] + \Delta^2 y_k[i] + \Delta^2 z_k[i]}}{c}, \quad (38)$$

$$\hat{a}_k[i] = \begin{cases} \theta = \arctan \frac{\sqrt{\Delta^2 x_k[i] + \Delta^2 y_k[i]}}{\Delta z[i]} \\ \phi = \arctan \frac{\Delta y_k[i]}{\Delta z[i]} \end{cases} \quad (39)$$

where $\Delta x_k[i] = x[i] - x_{a,k}$, $\Delta y_k[i] = y[i] - y_{a,k}$, $\Delta z_k[i] = z[i] - z_{a,k}$, then all \mathbf{y}_k at time step i can then be represented in a compact form as,

$$\mathbf{y}[i] = \mathbf{h}(s[i]) + \mathbf{m}[i] \quad (40)$$

where

$$\begin{aligned}\mathbf{y} &= [\mathbf{y}_1^T, \mathbf{y}_2^T, \dots, \mathbf{y}_K^T] \\ \mathbf{h} &= [\mathbf{h}_1^T, \mathbf{h}_2^T, \dots, \mathbf{h}_K^T] \\ \mathbf{m} &= [\mathbf{m}_1^T, \mathbf{m}_2^T, \dots, \mathbf{m}_K^T].\end{aligned}\quad (41)$$

$\mathbf{m} \sim \mathcal{N}(0, \mathbf{R})$ with a block diagonal covariance matrix $\mathbf{R} = \text{blkdiag}(\mathbf{R}_1, \mathbf{R}_2, \dots, \mathbf{R}_k)$. The estimation process is then expressed

by the following equations:

$$\hat{\mathbf{s}}^- [i] = \begin{bmatrix} 1 & 0 & 0 & \Delta t & 0 & 0 \\ 0 & 1 & 0 & 0 & \Delta t & 0 \\ 0 & 0 & 1 & 0 & 0 & \Delta t \\ 0 & 0 & 0 & 1 & 0 & 0 \\ 0 & 0 & 0 & 0 & 1 & 0 \\ 0 & 0 & 0 & 0 & 0 & 1 \end{bmatrix} * \hat{\mathbf{s}}^+ [i-1] + \mathbf{q}^+ [i] \quad (42)$$

$$\mathbf{P}^- [i] = \mathbf{A}\mathbf{P}^+ [i]\mathbf{A}^T + \mathbf{Q}[i] \quad (43)$$

For simplicity, the function of the target's movement has been modelled as a linear and discrete Wiener velocity model in equation (42) to denote the posteriori estimate and \mathbf{q} and \mathbf{P} are the process noise and the process covariance matrix representing the errors in the estimating process, respectively.

The update process with new measurement is given by

$$\mathbf{K}[i] = \frac{\mathbf{P}^- [i]\mathbf{H}[i]}{\mathbf{H}[i]\mathbf{P}^- [i]\mathbf{H}^T [i] + \mathbf{R}[i]} \quad (44)$$

$$\hat{\mathbf{s}}^+ [i] = \hat{\mathbf{s}}^- [i] + \mathbf{K}[i][\mathbf{Y}[i] - \mathbf{H}\mathbf{h}(\hat{\mathbf{s}}^- [i])] \quad (45)$$

$$\mathbf{P}^+ [i] = (\mathbf{I} - \mathbf{K}[i]\mathbf{H}[i])\mathbf{P}^- [i] \quad (46)$$

\mathbf{K} is the Kalman gain and \mathbf{I} is the identity matrix. In equations (43) - (46), \mathbf{H} and \mathbf{A} are both obtained from Jacobian matrices.

$$\mathbf{A}[i] = \frac{\partial \mathbf{f}[i]}{\partial \mathbf{s}[i]} \quad (47)$$

$$\mathbf{H}[i] = \frac{\partial \mathbf{h}[i]}{\partial \mathbf{s}[i]} \quad (48)$$

Finally, the estimated position of UN is obtained as $\mathbf{s}^+ [i] = (x^+ [i], y^+ [i], z^+ [i])$ with the update process covariance matrix $\mathbf{P}^+ [i]$.

3.2 Rectangular Array

At the smart phone, an $M \times N$ uniform rectangular array (URA) [20] consisting of patch antennas is employed for beam steering. The response of a URA can be written as

$$B(\psi_x, \psi_y) = e^{-j(\frac{N-1}{2}\psi_x + \frac{M-1}{2}\psi_y)} \sum_{m=0}^{M-1} \sum_{n=0}^{N-1} w_{nm}^* e^{j(n\psi_x + m\psi_y)} \quad (49)$$

where

$$\psi_x = \frac{2\pi}{\lambda} \sin \theta \cos \phi \quad (50)$$

$$\psi_y = \frac{2\pi}{\lambda} \sin \theta \sin \phi \quad (51)$$

and w_{nm} is the beamforming coefficient for the antenna at the n -th row and m -th column of the array. Each row has N elements, while each column has M elements, with $d_x = d_y = \lambda/2$ and θ and ϕ representing azimuth and elevation angles, respectively. The beam pattern of a uniform weighting rectangular array has relatively high side lobe levels. Therefore, the Hamming weight is applied to suppress the side lobes. The function for Hamming weighting is

$$\begin{aligned}w_x(n) = w_y(n) &= g_0 + g_1 \cos \frac{2\pi n}{N}, \\ n &= -\frac{N-1}{2}, \dots, \frac{N-1}{2}\end{aligned}\quad (52)$$

The coefficients g_0 and g_1 is determined for the array pattern to have a null at $\frac{1}{3}$. So the final function can be written as

$$\begin{aligned}w_x(n) = w_y(n) &= 0.54 + 0.46 \cos \frac{2\pi n}{N}, \\ n &= -\frac{N-1}{2}, \dots, \frac{N-1}{2}\end{aligned}\quad (53)$$

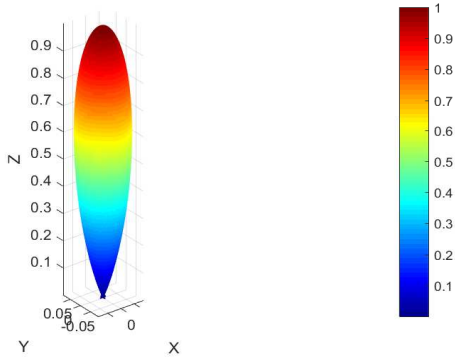


Fig. 2: Magnitude beam response of a 11×11 rectangular array with Hamming weight.

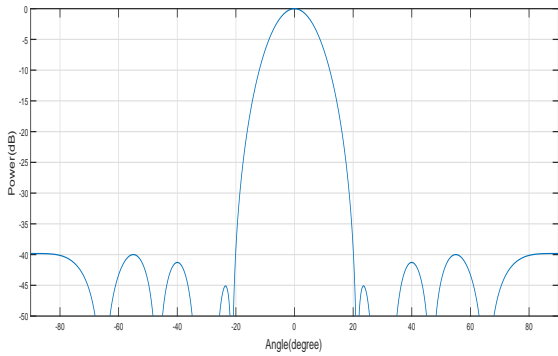


Fig. 3: A slice of the beam pattern of a 11×11 rectangular array with Hamming weight in logarithmic scale.

The beam pattern obtained by Hamming weight is provided in Figs. 2 and 3, which show a relatively good suppression of sidelobes.

In order to more effectively change the beam direction with the smart phone's movement, beam steering is employed instead of beam switching adopted in [11]. Beam steering can be achieved by adjusting the phase shift variables, of which θ_0 and ϕ_0 are the desired steering angles calculated from the LoS vector.

$$B_0(\psi_x, \psi_y) = e^{-j(\frac{N-1}{2}\psi_x + \frac{M-1}{2}\psi_y)} \sum_{m=0}^{M-1} \sum_{n=0}^{N-1} w_{nm}^* e^{j(n(\psi_x + \beta_x) + m(\psi_y + \beta_y))} \quad (54)$$

where

$$\beta_x = \frac{2\pi}{\lambda} \sin \theta_0 \cos \phi_0 \quad (55)$$

$$\beta_y = \frac{2\pi}{\lambda} \sin \theta_0 \sin \phi_0 \quad (56)$$

4 The Proposed Tracking Algorithm

The proposed overall tracking algorithm is illustrated in the flowchart in Fig. 4. The solid line denotes the algorithm operating at the AN side, while the dash line denotes the network operation. The proposed technique incorporates the 5G cellular network and the individual smart phone as a whole to aid the beam tracking operation.

When the UN enters the coverage of a 5G network, it will synchronize with the AN at the first place and the uplink signal will be processed for beam training to initialize localization tracking. The DoA and ToA EKF tracking algorithm will operate and keep running through the whole process of the communication. The location

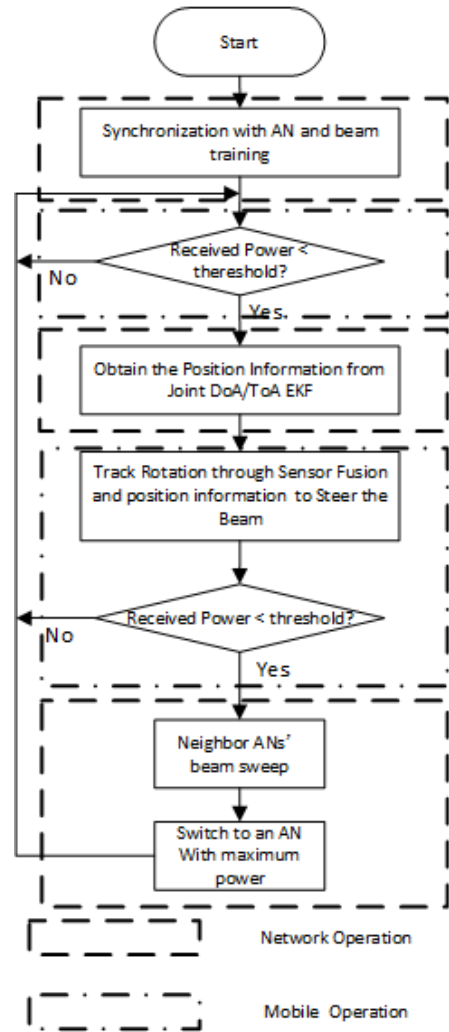


Fig. 4: Flowchart of proposed beam tracking process.

information obtained from joint DoA/ToA will be applied for sensor fusion to establish and maintain the beam alignment. If the received signal power drops below a predefined threshold value, the network system will trigger neighbor ANs to scan for the UN's beam and one AN with maximum power link to the UN will be established. The whole process will be performed again to maintain the quality of the communication link.

5 Simulation Results

In this section, the performance of the proposed algorithm is examined in three different scenarios. The first one is self-rotation with a fixed UN position and one AN, the second one is self-rotation with straight-line movement of the UN in a short distance and one AN, and the third one is self-rotation with straight-line movement of the UN along a long distance and six ANs. For simplicity, the multipath effect and the transmission and handover time are not considered in this paper.

For all the scenarios, the setting of self-rotation tracking simulation is the same. The initial state is 0 for all the sensors and the gyroscope error magnitude β is set to be 0.1 [15]. The delay of sensor measurements can be ignored as it is at the order of nanoseconds. The delay of beam steering is picoseconds and can be ignored too [21], and the operation time is 30s. The self-rotation tracking result for the first 10 seconds is shown in Fig. 5. The RMSEs of yaw-roll-pitch angle are 1.1530° , 0.5920° and 0.4937° for the self-rotation tracking results, respectively. According to [22], the result indicates

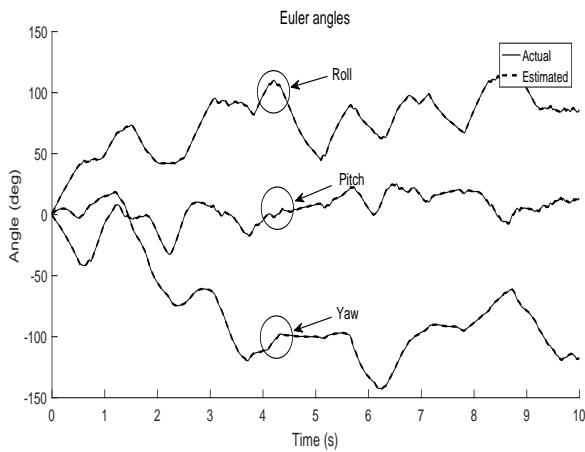


Fig. 5: Self-rotation tracking result.

that the self-rotation tracking algorithm has achieved a high level of accuracy.

In the first scenario, the UN stands at a fixed position with a pre-defined self-rotation rate and one AN. The location tracking EKF employed here is initialized with a coarse estimate obtained from GPS, DoA or some other commercial position systems, since the initial value only has a very limited impact on the following tracking process [18]. The update period is $T_t = 167.3\mu s$ [23]. The target starts at state $s = [0 \ 0 \ 0 \ 1 \ 0 \ 0]^T$. Within the update cycle, the noise variance magnitude of DoA and ToA is set to be 0.1. The update process follows the equations from (42) to (46). The tracking result for the first 1000 iterations is shown in Fig. 6a, with n being the update index number. We can see that the location of UN is estimated at around (2.5,0,0.7) and the calculated RMSE is 0.9603.

The location information of UN is used in the following beam tracking process and the beam tracking results are presented in Fig. 6b for the three rotation angles. We can see that for the case without tracking, the signal power has dropped to a very low level destroying the communication link entirely. In contrast, the sensor-aided tracking method provides continuous high signal power during the process. In Fig. 7, the average signal power with different different noise variance magnitude in dB is presented, the signal power has always stayed above -2dB from -40dB to 0dB.

In the second scenario, the UN moves along a 5-metre straight line at a constant speed for 10s and communicates with one AN. The AN is placed at the middle of the trajectory at position (5, 1, 5). A 3-D location tracking result is shown in Fig. 8a. It is clear that, the localization is quite accurate in 5-metre movement with an RMSE of 0.9612.

It can be seen from Figs. 8b and 8c that without tracking the directions of the beam point to everywhere and with tracking the beams have been focused towards the AN. Note that for convenience to visualize, only some sampled points are displayed in Figs. 8b and 8c. The received signal power is shown in Fig. 8d, and the average signal power with different noise variance magnitude in dB is shown in Fig. 9. We can see that the received signal power stays at a high level to keep the connection in the process even with a high noise variance.

In scenario three, the UN moves along a 30 metres straight line at a constant speed for 30 seconds with 6 ANs. During the process, the UN switches the connection with the AN every 5 metres. And the result and demonstration of the process is shown in Fig. 10a at an RMSE of 0.9625 metres. It can be seen from the comparison between Figs. 10b and 10c that the beam of the tracking aided UN has always been pointing to the right AN, while the beam direction without tracking looks like a random process. The received signal power also stays at a high level in Fig. 10d and Fig. 11 with different noise variances, all above -0.06dB.

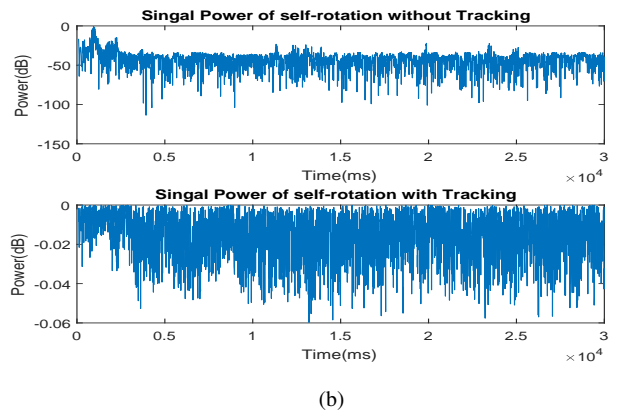
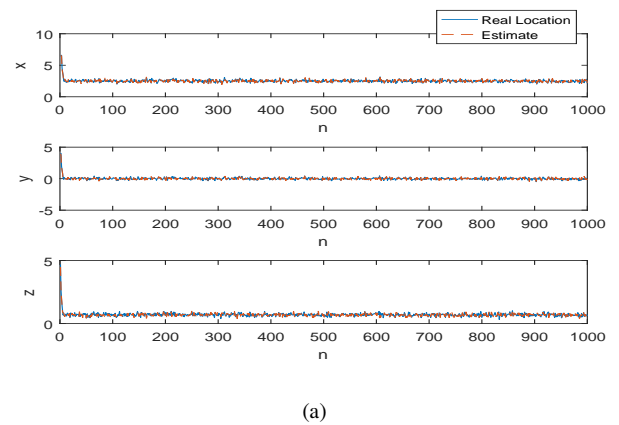


Fig. 6: (a) Location tracking result, and (b) signal power with and without tracking for scenario 1.

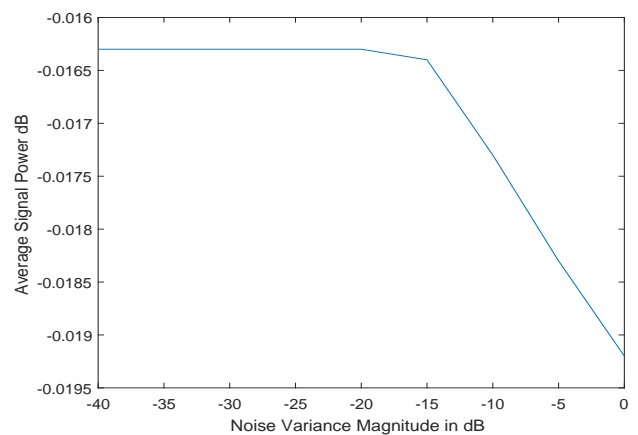
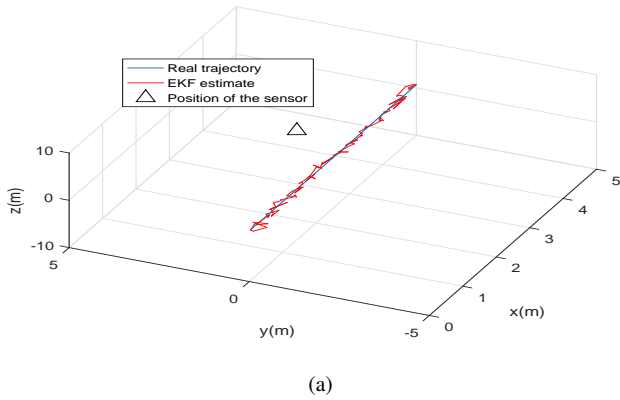


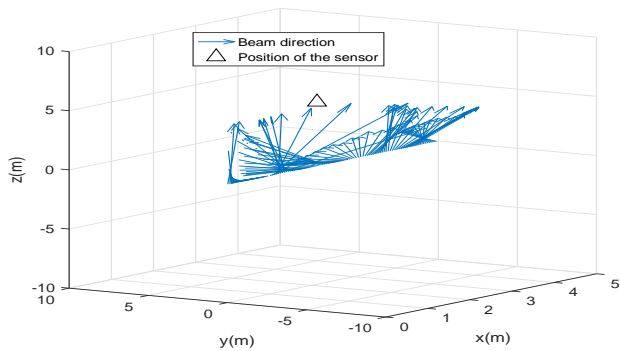
Fig. 7: Average signal power with different noise variance magnitude in dB for scenario 1.

6 Conclusion

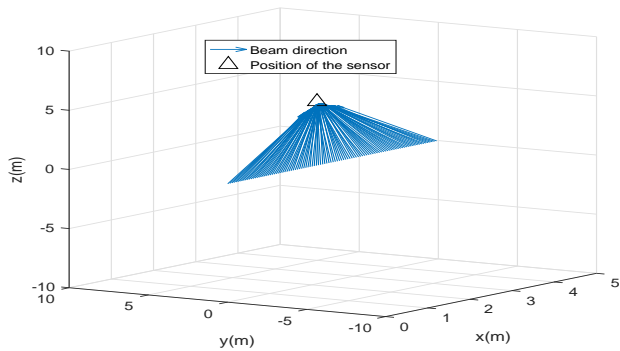
A new 3-D millimetre wave beam tracking method with network level implementation has been proposed. There are two parts in the proposed method: one is the self-rotation tracking using three embedded smart phone sensors based on a gradient descent algorithm; the other one is location tracking using a combination of DoA and ToA information through extended Kalman filtering. The performance of the proposed method has been demonstrated through three typical scenarios: one is with a fixed UN location and one AN involved, while the other two are with a steady straight-line movement, but with different number of ANs involved.



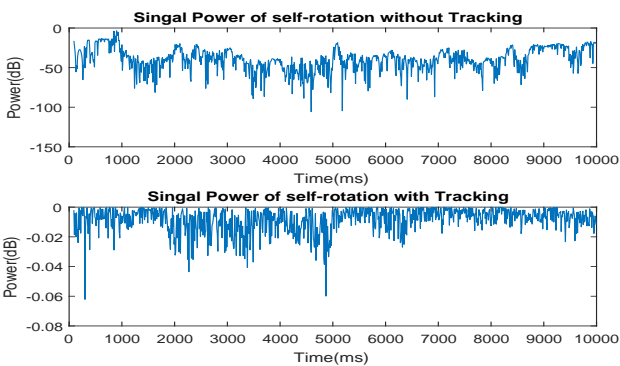
(a)



(b)



(c)



(d)

Fig. 8: (a) Location tracking result in 2D, (b) UN beam directions without tracking, (c) UN beam directions with tracking, and (d) signal power with and without tracking for scenario 2.

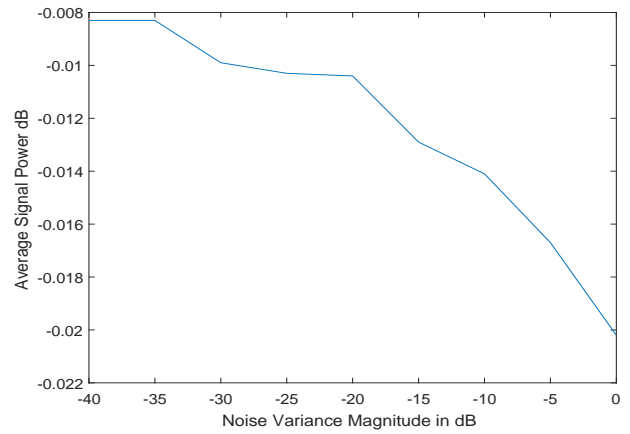


Fig. 9: Average signal power with different noise variance magnitude in dB for scenario 2.

7 References

- Huawei. "5G: A technology vision (white paper)", 2013. Available: <http://www.huawei.com/5gwhitepaper/>.
- D. Dardari, P. Closas, and Petar M. Djurić. Indoor tracking: Theory, methods, and technologies. *IEEE Transactions on Vehicular Technology*, 64(4):1263–1278, Apr. 2015.
- J. Medbo, I. Siomina, A. Kangas, and J. Furuskog. Propagation channel impact on LTE positioning accuracy: A study based on real measurements of observed time difference of arrival. In *IEEE 20th International Symposium on Personal, Indoor and Mobile Radio Communications*, volume 4, 2009.
- H. Liu, Y. Gan, J. Yang, S. Sidhom, Y. Wang, Y. Chen, and F. Ye. Push the limit of wifi based localization for smartphones. In *Proceedings of the 18th Annual International Conference on Mobile Computing and Networking*, volume 11, pages 305–316. ACM, 2012.
- J. Werner, M. Costa, A. Hakkarainen, K. Leppanen, and M. Valkama. Joint user node positioning and clock offset estimation in 5G ultra-dense networks. In *IEEE Global Communications Conference (GLOBECOM)*, pages 1–7. IEEE, 2015.
- J. Werner, J. Wang, A. Hakkarainen, D. Cabric, and M. Valkama. Performance and cramer-rao bounds for DoA/RSS estimation and transmitter localization using sectorized antennas. *IEEE Transactions on Vehicular Technology*, 65(5):3255–3270, 2016.
- X. Cheng, D. Zhu, S. Zhang, and P. He. Tracking positioning algorithm for direction of arrival based on direction lock loop. *Future Internet*, 7(3):214–224, 2015.
- M. Giordani, M. Mezzavilla, A. Dhananjay, S. Rangan, and M. Zorzi. Channel dynamics and SNR tracking in millimeter wave cellular systems. (8), Apr. 2016.
- M. Park and Helen K. Pan. Effect of device mobility and phased array antennas on 60 GHz wireless networks. In *Proceedings of the ACM International Workshop on mmWave Communications: From Circuits to Networks*, pages 51–56. ACM, 2010.
- Y. Inoue, Y. Kishiyama, Y. Okumura, J. Kepler, and M. Cudak. Experimental evaluation of downlink transmission and beam tracking performance for 5G mmW radio access in indoor shielded environment. In *Personal, Indoor, and Mobile Radio Communications (PIMRC), IEEE 26th Annual International Symposium on*, pages 862–866. IEEE, 2015.
- D. Shim, C. Yang, J. Kim, J. Han, and Y. Cho. Application of motion sensors for beam-tracking of mobile stations in mmwave communication systems. *Sensors*, 14(10):19622–19638, 2014.
- Z. Qi and W. Liu. Three-dimensional millimetre wave beam tracking based on handset mems sensors with extended kalman filtering. In *Radio Propagation and Technologies for 5G*, pages 1–6. IET, 2016.
- B. Barshan and H. F. Durrant-Whyte. Inertial navigation systems for mobile robots. *IEEE Transactions on Robotics and Automation*, 11(3):328–342, 1995.
- E. Foxlin. Inertial head-tracker sensor fusion by a complementary separate-bias kalman filter. In *Virtual Reality Annual International Symposium, 1996., Proceedings of the IEEE 1996*, pages 185–194. IEEE, 1996.
- A. Madgwick, S. and Harrison and R. Vaidyanathan. Estimation of imu and marg orientation using a gradient descent algorithm. In *Rehabilitation Robotics (ICORR), 2011 IEEE International Conference on*, pages 1–7. IEEE, 2011.
- M. D. Jiang, Y. Li, and W. Liu. Properties of a general quaternion-valued gradient operator and its application to signal processing. *Frontiers of Information Technology & Electronic Engineering*, 17:83–95, February 2016.
- Gregory G. Slabaugh. Computing euler angles from a rotation matrix. Retrieved on August, 6(2000):39–63, 1999.
- D. Simon. *Optimal State Estimation: Kalman, H Infinity, and Nonlinear Approaches*. Hoboken, N.J.: Wiley-Interscience, 1st edition, Jun 2006.
- R.G. Valenti, I. Dryanovski, and J. Xiao. Keeping a good attitude: A quaternion-based orientation filter for imus and margs. *Sensors*, 15(8):19302–19330, 2015.
- W. Liu and S. Weiss. *Wideband Beamforming: Concepts and Techniques*. John Wiley & Sons, Chichester, UK, 2010.
- M. Longbrake. True time-delay beamsteering for radar. In *Aerospace and Electronics Conference (NAECON), IEEE National*, pages 246–249. IEEE, 2012.

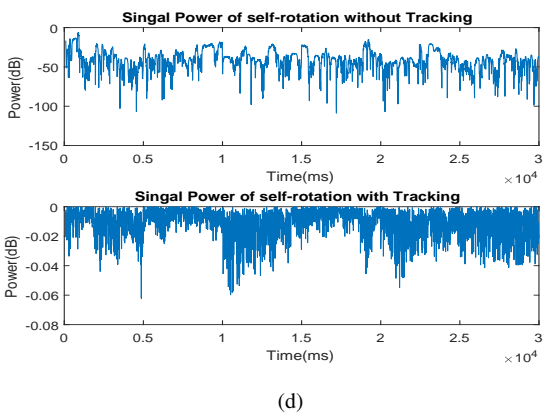
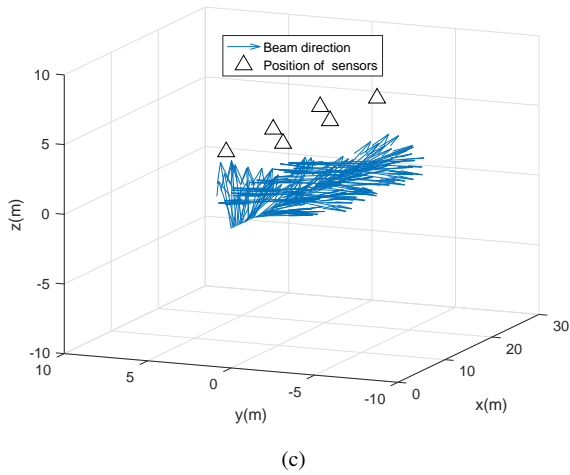
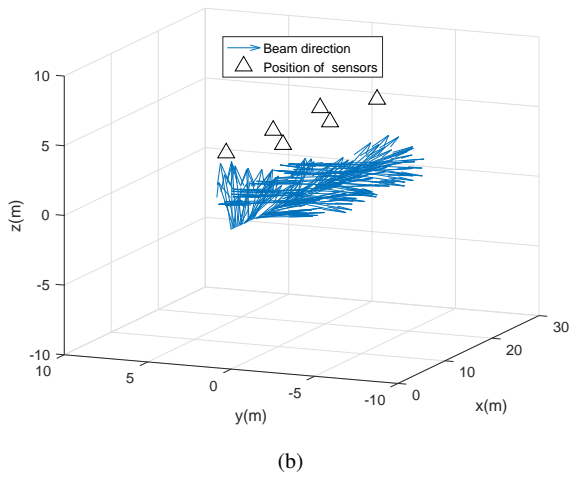
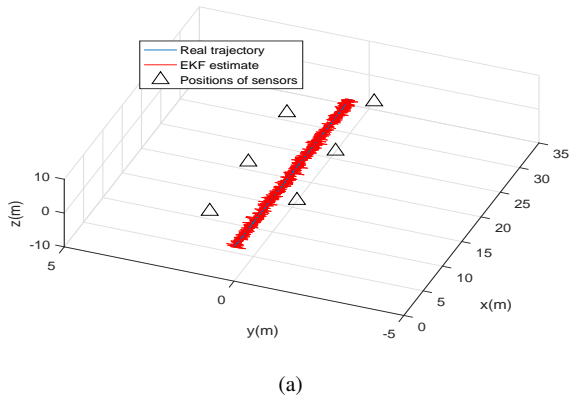


Fig. 10: (a) Location tracking result in 2D, (b) UN beam directions without tracking, (c) UN beam directions with tracking, and (d) signal power with and without tracking for scenario 3.

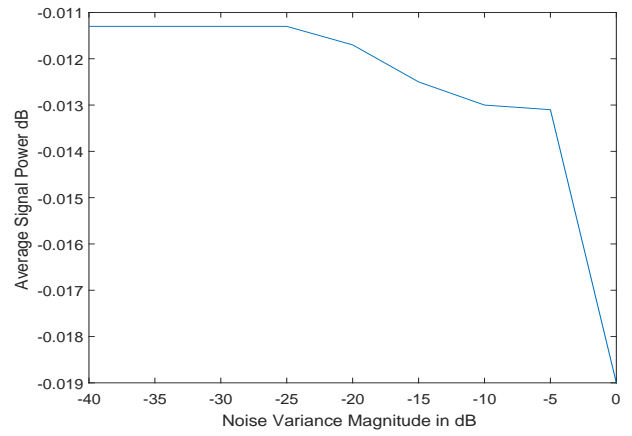


Fig. 11: Signal power with different noise variance magnitude in dB for scenario 3.

- 22 J. Hartikainen, A. Solin, and S. Särkkä, Simo. Optimal filtering with kalman filters and smoothers. *Department of Biomedica Engineering and Computational Sciences, Aalto University School of Science, 16th August, 2011.*
- 23 P. Kela, M. Costa, J. Salmi, K. Leppanen, J. Turkka, T. Hiltunen, and M. Hronec. A novel radio frame structure for 5G dense outdoor radio access networks. In *IEEE 81st Vehicular Technology Conference (VTC Spring)*, pages 1–6. IEEE, 2015.